Supplementary Information for

Hybrid aeromaterials for enhanced and rapid volumetric photothermal response

*Lena M. Saure[1], Niklas Kohlmann[2], Haoyi Qiu[1], Shwetha Shetty[3], Ali Shaygan Nia[4], Narayanan Ravishankar[3], Xinliang Feng[4], Alexander Szameit[5,6], Lorenz Kienle[2,7], Rainer Adelung[1,7], Fabian Schütt[1,7]***

[1] Functional Nanomaterials and [2] Synthesis and Real Structure, Department for Materials Science, Kiel University, Kaiser Str. 2, 24143 Kiel, Germany
* fas@tf.uni-kiel.de

[3] Materials Research Centre, Indian Institute of Science, Bangalore, Karnataka, IN 560012, India

[4] Department of Chemistry and Food Chemistry, Center for Advancing Electronics Dresden (cfaed), Dresden University of Technology, 01062 Dresden, Germany

[5] Department for Physics and [6] Department of Life, Light & Matter, University of Rostock, 18059 Rostock, Germany

[7] Kiel Nano, Surface and Interface Science KiNSIS, Kiel University, Christian-Albrechts-Platz 4, 24118 Kiel, Germany

This PDF file includes:

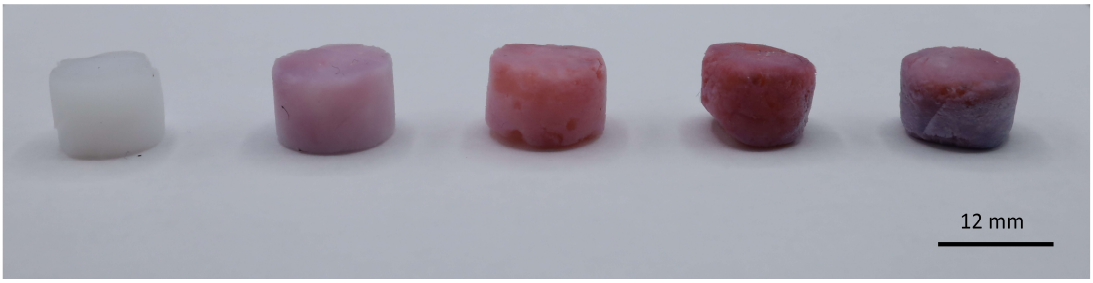

Figure S1. Aeroglass (AG) functionalized with increasing concentration (from left to right) of gold nanoparticles.

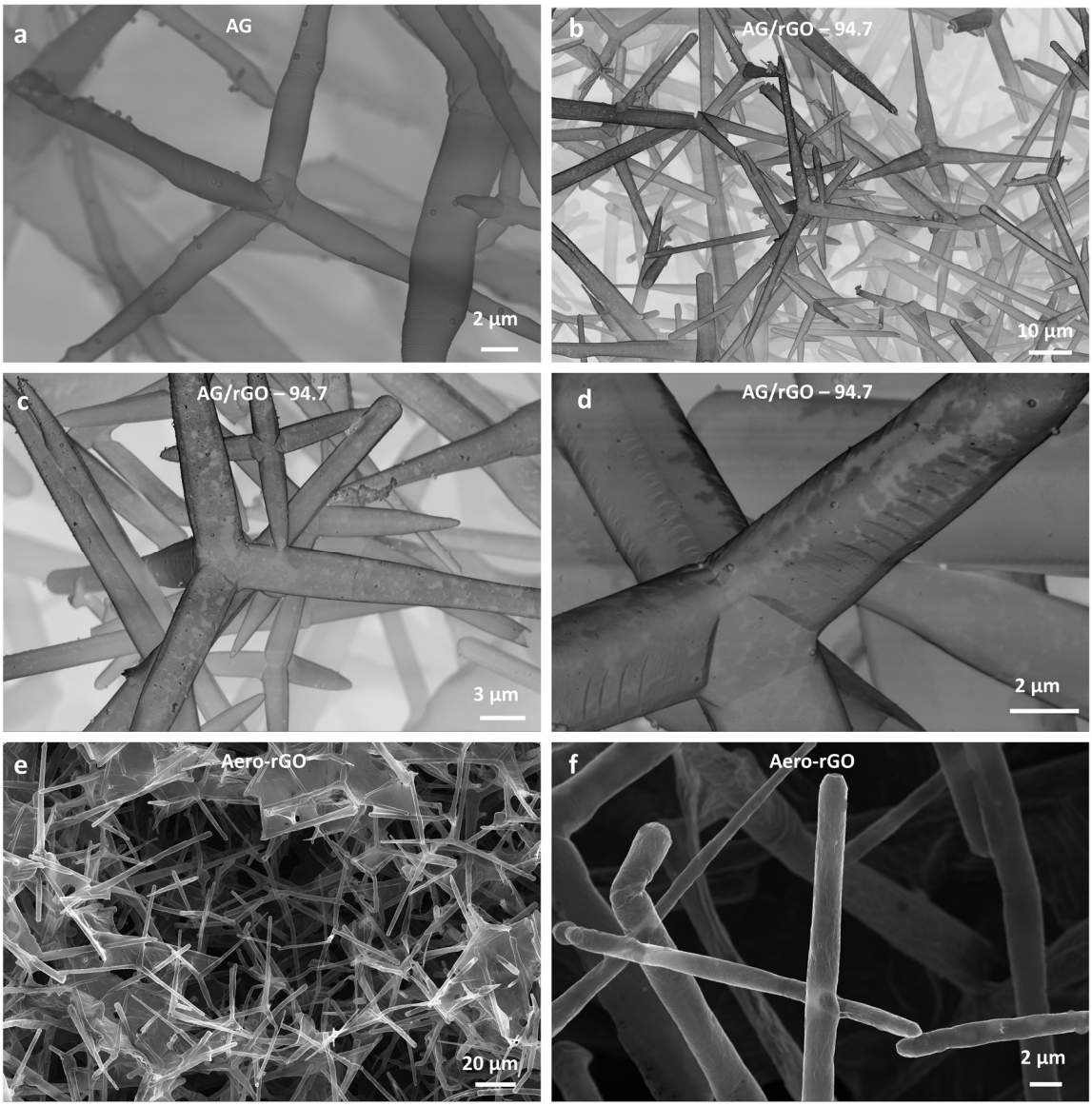

Figure S2. Detailed scanning electron microscopy (SEM) characterization of (a) pristine aeroglass (AG), (b-d) AG/rGO with volumetric loading of 94.7 µg cm^{-3} rGO with increasing magnification. The stained surface of the SiO_2 microtubes indicates the homogeneous coating with rGO flakes. (e-f) SEM images of Aero-rGO with increasing magnification.

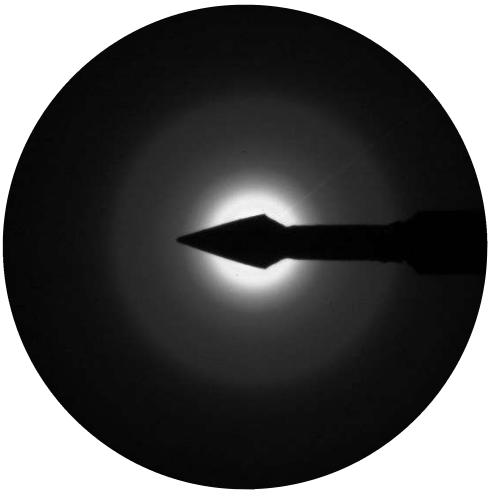

Figure S3 Diffraction pattern recorded by TEM of pristine aeroglass revealing the amorphous character of SiO_2 microtubes.

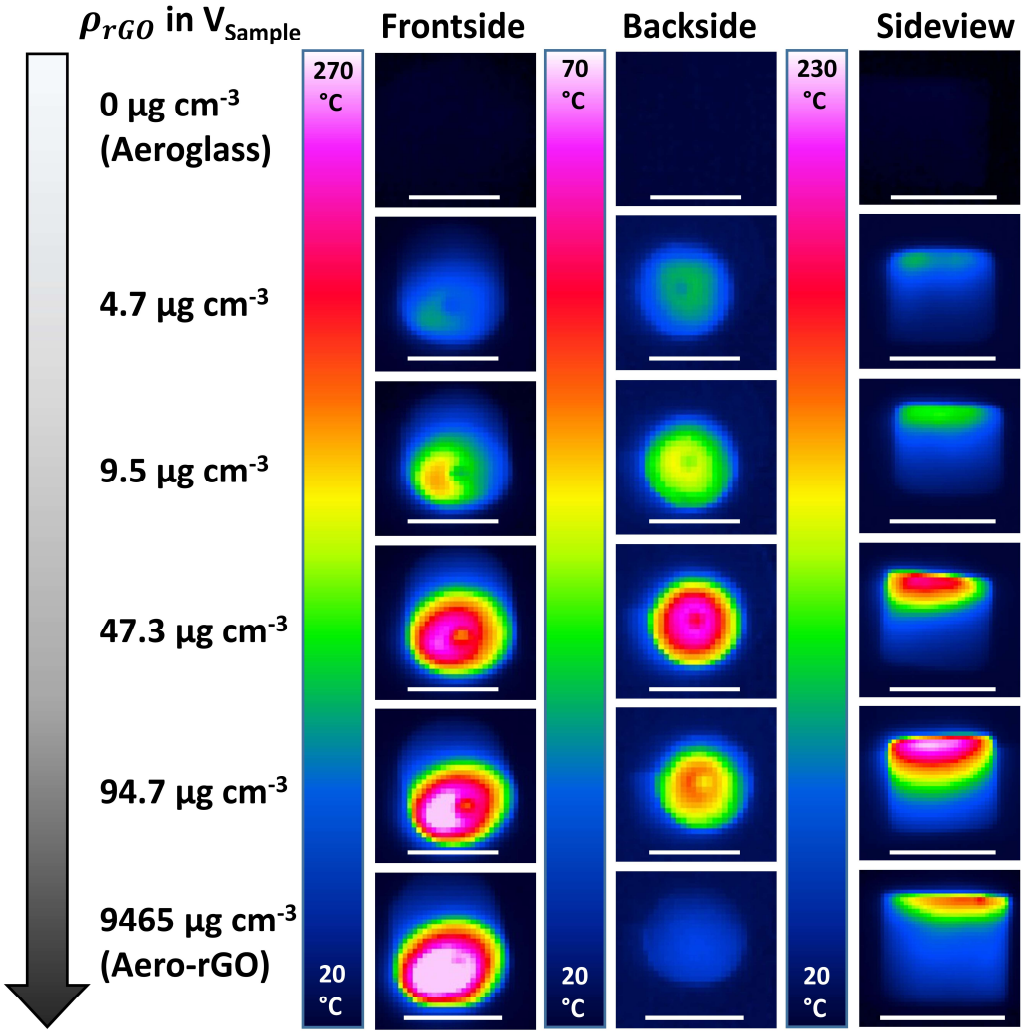

Figure S 4. Infrared images of hybrid aeroglass with increasing volumetric rGO loading from top to bottom. Images were recorded from the fontside (illumination side), backside, and the sideview of the samples for an illumination for 1 s with an irradiance of 1.67 W cm^{-2}. Scale bar is 12 mm.

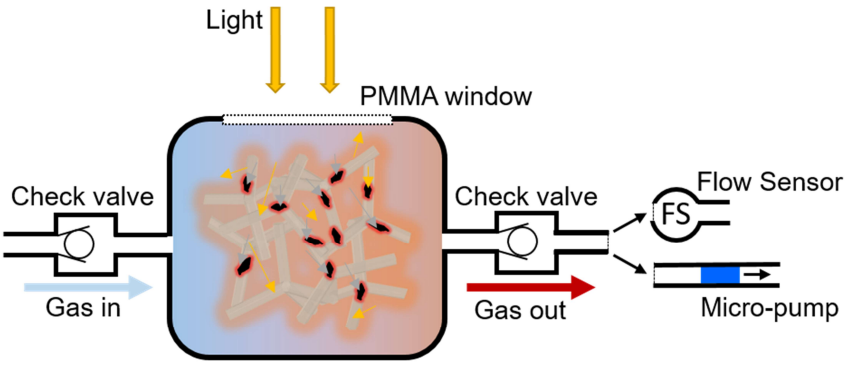

Figure S5. Schematic of air-tight chamber with multiple connection options.

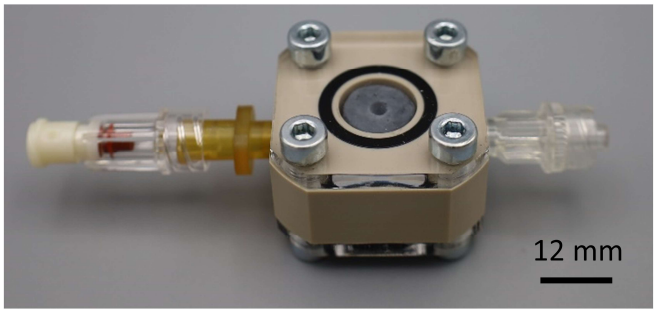

Figure S6. Photograph of air-tight chamber containing a AG/rGO sample.

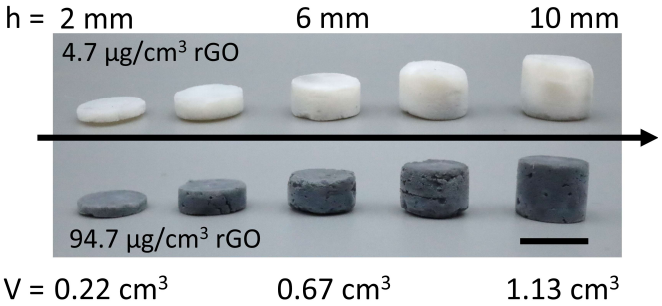

Figure S7. Photograph of AG/rGO-4.7 and AG/rGO-94.7 with varying sample dimensions. Scale bar is 12 mm.

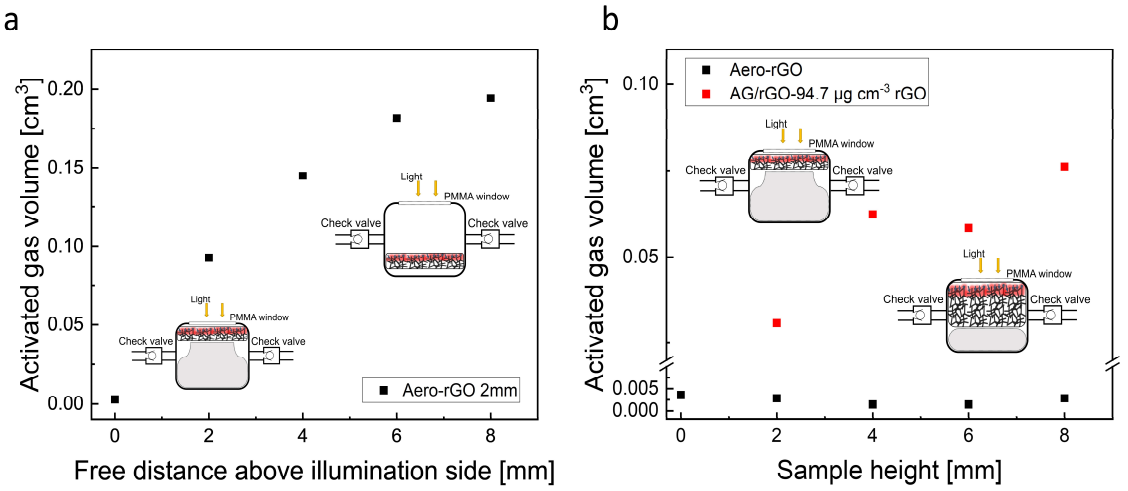

Figure S8. Activated gas volume of (a) Aero-rGO with 2mm sample height. The sample was placed in an air-tight chamber whereby the distance to the polymethylmethacrylate window was varied from 0 mm to 8mm. This resulted in varying free volumes above the illumination side, as demonstrated with the schematic insets. With increasing free volume above the illumination side, the activated gas saturates. (b) Activated gas volume for Aero-rGO and AG/rGO-94.7 with increasing sample height and a distance of 0 mm to the polymethylmethacrylate window. In this configuration only the volumetric gas activation by the photothermal effect is measured, demonstrating that only the surface region contributes to the gas activation. The insets show the position of the samples in the air-tight chamber and the heated surface region for Aero-rGO. In contrast, AG/rGO-94.7 shows an increase in gas volume with sample height, indicating a volumetric photothermal conversion.

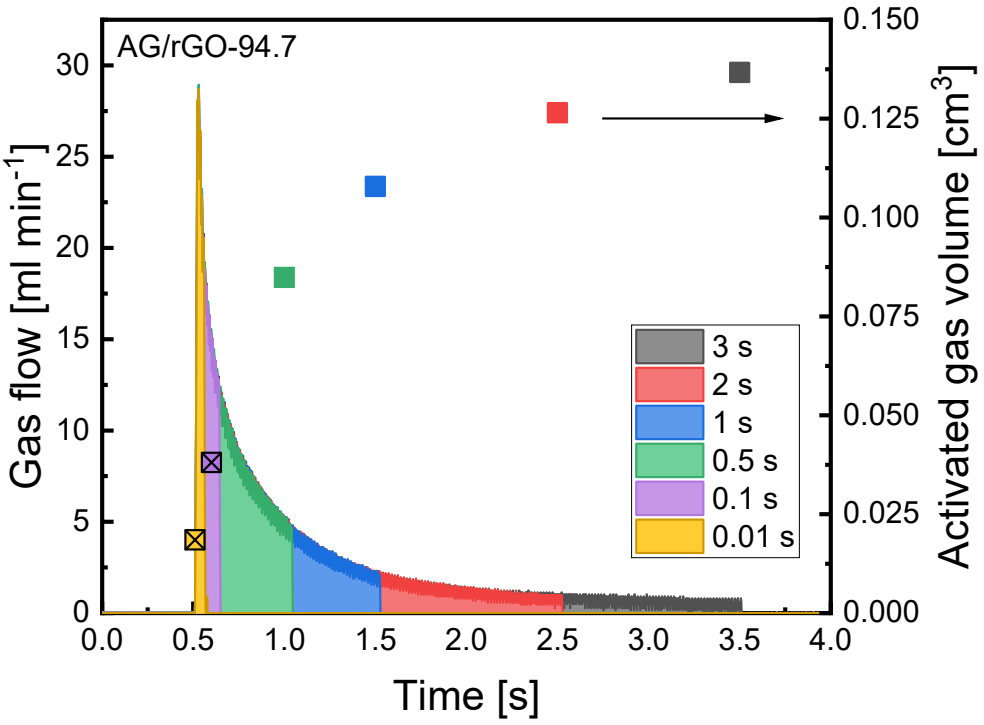

Figure S9. Gas flow generated by AG/rGO-94.7 illuminated with varying times ranging between 0.01 s and 3 s.

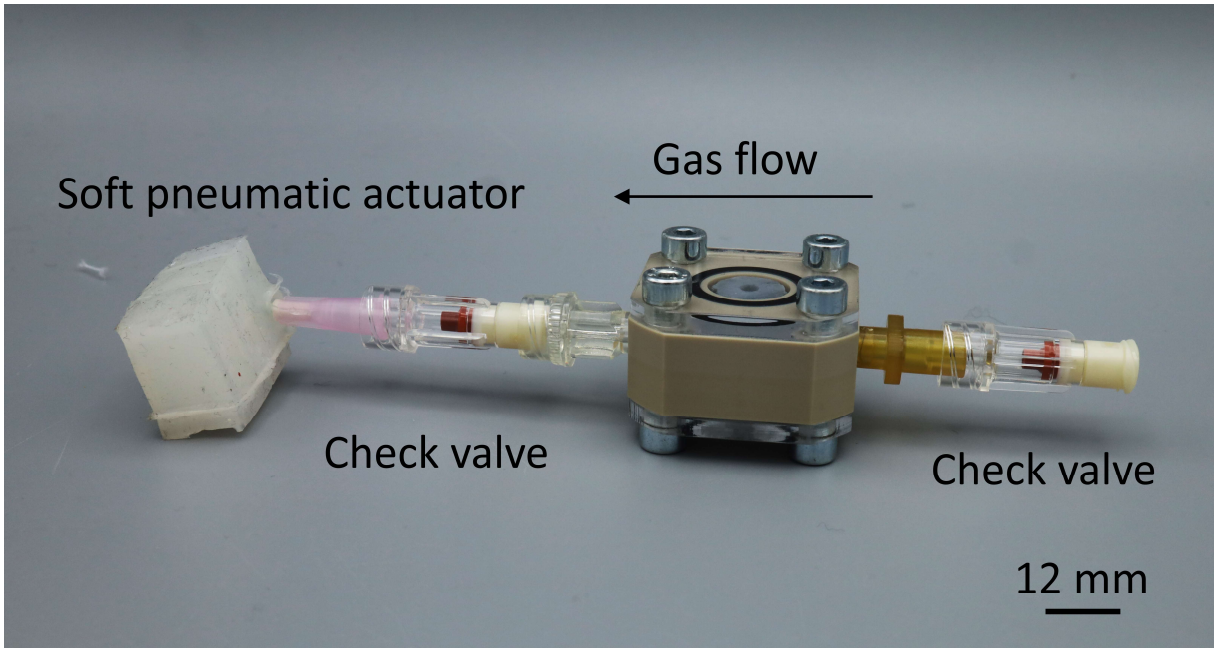

Figure S10. Set-up for untethered soft pneumatic actuator that can be controlled by light. The check valves allow a directional gas flow upon illumination of the aeromaterial transducer resulting in a step-wise bending of the soft pneumatic actuator.

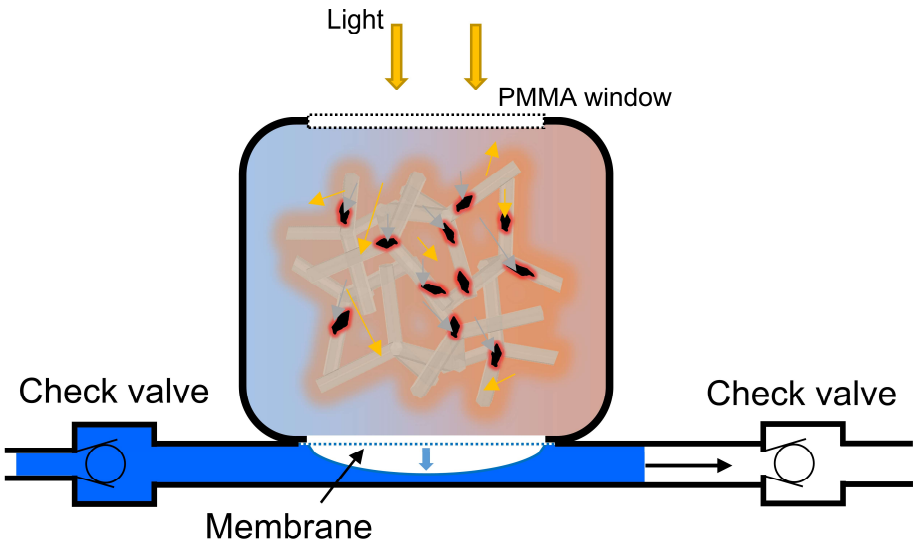

Figure S11. Schematic concept of wireless light-powered membrane pump. Illumination of AG/rGO in an enclosed chamber results in a pressure rise that causes a repeatable straining of the flexible membrane.

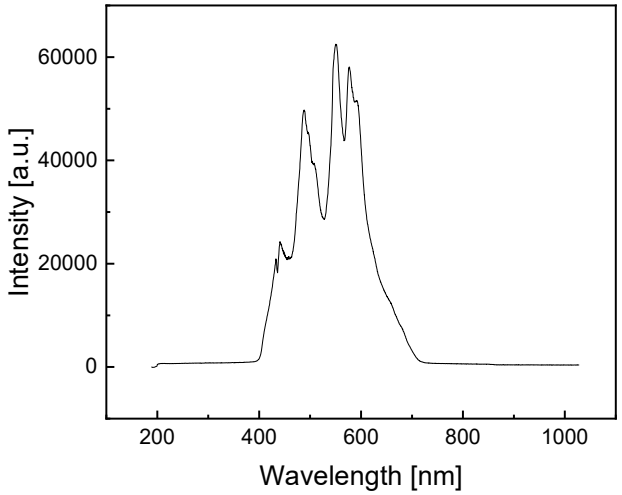

Figure S 12. Spectrum of beamer (Acer, DLP Projector, DNX0906).

Supplementary Note 1 - TEM investigation of aeroglass

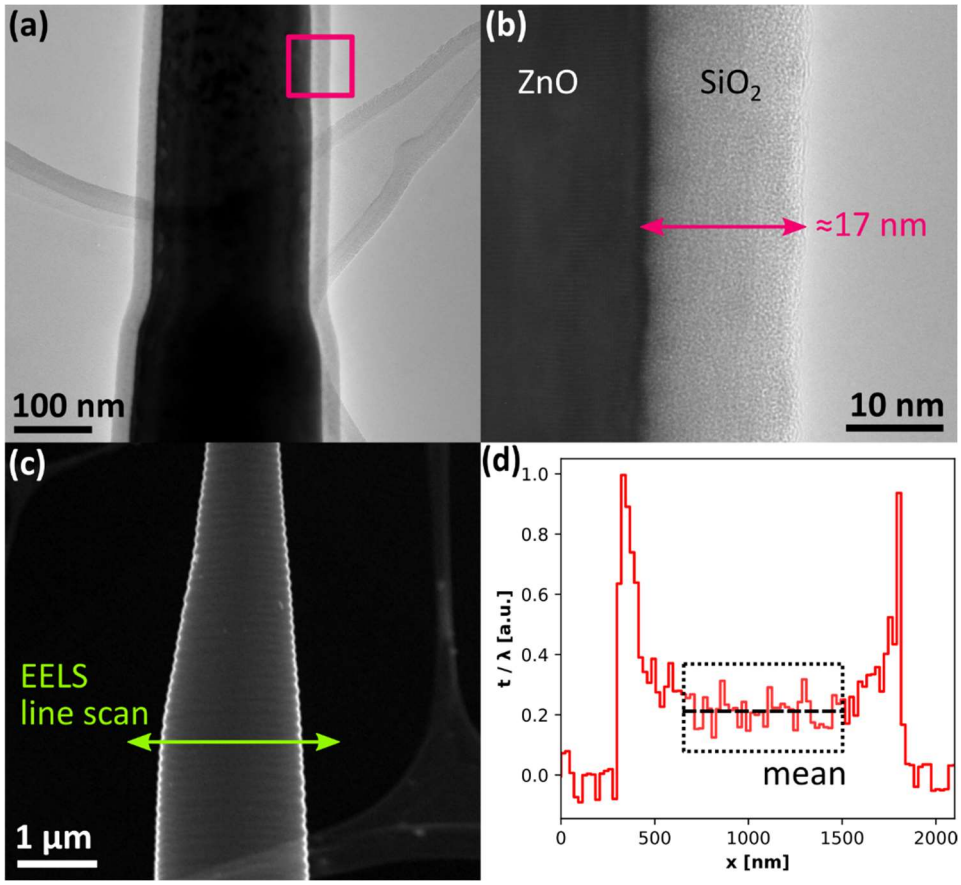

Figure S13. (a) TEM image of a ZnO tetrapod arm coated with a thin SiO_2 layer under identical parameters as for AG fabrication showing a homogenous layer thickness. (b) HRTEM micrograph of the area marked in (a). The SiO_2 layer can clearly be distinguished from the ZnO due to mass thickness and diffraction contrast. (c) HAADF-STEM image of an AG microtube. (d) Relative thickness profile of the microtube from (c) along the indicated line scan path. The (relative) wall thickness of the tube is determined by taking the mean from the indicated area.

TEM investigation of AG and AG/rGO was carried out both to reveal its general properties and functionalization (as shown in the main manuscript) as well as to determine the SiO_2 wall thickness. In order to determine the SiO_2 wall thickness two complementary approaches can be used. First, the wall thickness can be determined directly by fabricating specimens that are coated with SiO_2 in an identical process used for AG synthesis but without removing the ZnO. Accordingly, ZnO tetrapods coated with a SiO_2 layer of identical thickness to the corresponding AG wall thickness are obtained, see **Figure S13a**. The SiO_2 layer thickness can then directly be determined using HRTEM due to the strong contrast between the crystalline ZnO and the amorphous SiO_2, see **Figure S13b**. By investigating multiple tetrapod arms and locations an

average layer thickness of 17 +- 0.5 nm is found. The uncertainty is given by the standard error of the measurements.

The second approach can be applied to AG directly. By utilizing the electron energy loss spectroscopy (EELS) log ratio method[1] the relative thickness in electron beam direction can be determined in multiples of the inelastic electron mean free path (IEMFP). Using appropriate approximations for the IEMFP [1,2], the absolute thickness can then be subsequently obtained. If the EELS log ratio method is combined with STEM EELS, localized thickness information can be gathered. Performing line scans across a hollow AG microtube as shown in **Figure S13c**, then yields the thickness profile across the AG microtube given in **Figure S13d**. Taking the mean of the center area of approximately constant layer thickness, due to the curvature of the tube, and dividing by a factor of two taking into account that the electron beam passes through the SiO_2 layer twice, yields the relative layer thickness. Measuring multiple tubes and positions results in a relative AG wall thickness of 0.11 +- 0.025 IEMFP. Using the approximation given by Malis et al.[1] results in an IEMFP of 143.5 nm while the formula from Iakoubovskii et al.[2] using a mass density of 2.0 g cm^{-3} for stoeber silica [3] results in an IEMFP of 197 nm. Multiplying the relative thickness determined via EELS log ratio with the calculated IEMFPS for (stoeber) SiO_2 yield the absolute wall thickness of 15.8 +- 0.4 nm using Malis et al.[1] and 21.7 +- 0.5 nm using [2,3]. The deviation between the two thickness values denotes a typical shortcoming of the EELS log ratio method where the accuracy of absolute thicknesses is dominated by the uncertainty in the IEMFP, which is for most cases not precisely known. In this investigation, however, the thickness value of 15.8 +- 0.4 nm determined via the EELS log ratio method using the IEMFP calculation from Malis et al.[1] is remarkably close to the directly determined layer thickness of 17 +- 0.5 nm. If multiple specimens of AG or different layer thickness were to be measured the direct thickness value could be used to calibrate the EELS log ratio measurements using an effective experimental IEMFP. In this case an IEMFP of 154.5 nm would correspond to the directly determined layer thickness.

The observations and conclusions require that the SiO_2 layer thickness is not changed during ZnO removal in the AG fabrication process. Both the chemical inertness of SiO_2 towards the etching agent as well as the closely matching thickness values support this assumption.

Supplementary Note 2 – Comment on UV-vis spectroscopy

UV-vis spectroscopy was carried out for pristine AG, AG/rGO with varying volumetric loading of rGO (4.7 µg cm^{-3} rGO, 9.47 µg cm^{-3} rGO, 47.3 µg cm^{-3} rGO and 94.7 µg cm^{-3} rGO), see **Figure 2f** in main manuscript, as well as for pristine Aero-rGO (9465 µg cm^{-3} rGO), see **Figure S14**. The measurements were conducted in water to avoid measurement artefacts by strong light scattering. The index of refraction of water is close to that of SiO_2, therefore almost no light scattering occurs. In contrast, when measuring aeroglass structures in air, nearly no light would reach the detector, as the samples scatter light to all space angles. Pristine AG shows low absorbance for 400 nm to 500 nm with a decreasing trend for higher wavelengths. It should be noted, that although the measurements were conducted in water to avoid scattering, this might still cause a deviation of the absorbance values. AG/rGO-4.7 shows a slightly higher absorbance over the measured wavelength range compared to pristine AG. In contrast, AG/rGO-94.7 rGO shows a strongly enhanced absorbance over the entire wavelength range with highest absorbance for 450 nm to 550 nm and a decreasing trend towards higher wavelengths and the near infrared range (NIR). The absorbance of AG/rGO with intermediate degree of functionalization shows the same trend with absorbance values in between the values for low and high loadings of rGO. For comparison, the absorbance of pristine Aero-rGO was measured as well. The result is shown in **Figure S14**. All light is directly absorbed and almost no light reaching the detector.

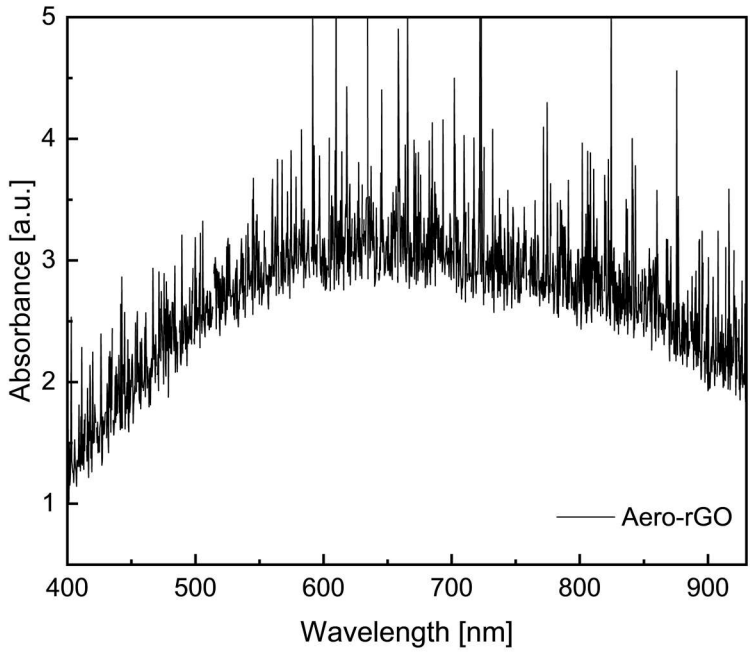

Figure S14. UV-vis absorption spectra of Aero-rGO.

Supplementary Note 3 – Light scattering in aeroglass

Pristine AG (**Figure S15a**) shows a unique open porous hierarchical structure with different sized features such as microsized voids (100-300 µm), which are much larger than the wavelength of visible light, the diameter of the microtubes (1-3 µm), which is in the same order of magnitude as the wavelength of visible light, and the nanoscopic wall thickness, which is much smaller than the wavelength of visible light, as schematically shown in **Figure S15b,** thus, creating an optical disorder system in which the nanoscopic wall thickness provides scattering centers for Rayleigh type light scattering.[4] Scattering occurs randomly in any space direction. Light impinging on the structure can be scattered multiple times before leaving the structure, thus, acting as a diffuser for light, as shown in **Figure S15c**.

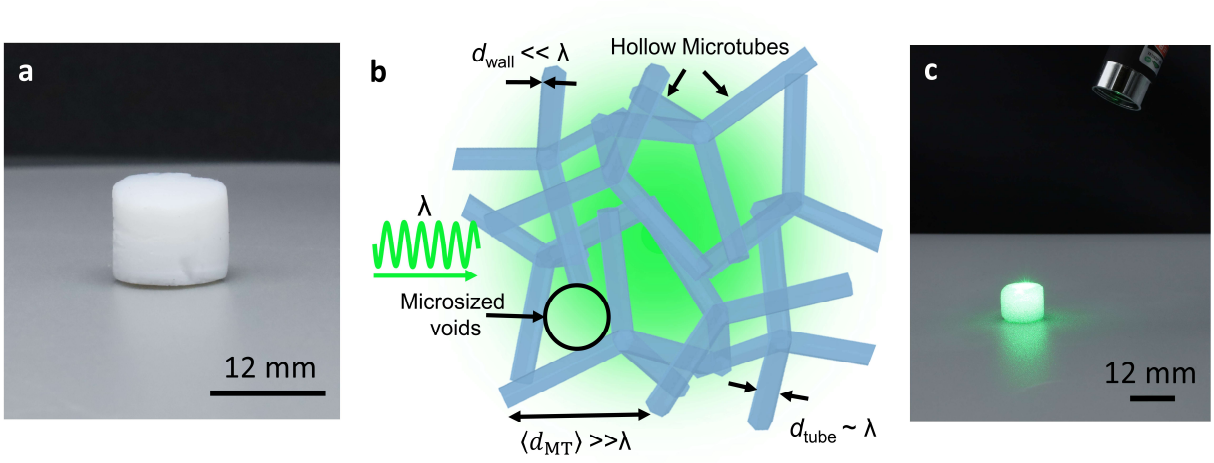

Figure S15. (a) Photograph of pristine AG showing optically white appearance. (b) Schematic of microstructure composed of hollow interconnected microtubes with hierarchical features sizes. (c) Photograph of AG illuminated with a green laser, scattering the light in any space direction.

Supplementary Note 4 – Calculation of volumetric specific heat capacity

The volumetric specific heat capacity of highly porous and low density materials is difficult to determine with standard methods as e.g. the laser flash method. Therefore, the volumetric specific heat capacity was calculated as a rough estimate based on the molar specific heat capacity of amorphous SiO_2: $c \approx 50\ J\ mol^{-1}\ K^{-1}$ [5]

The specific heat capacity of SiO_2 is calculated by

$$c_p = c * M, \tag{S1}$$

with M being the molar mass of SiO_2. As the molar mass changes for different crystallinities, we here assume a value of $M = 60.1\ g\ mol^{-1}$, hence, $c_p = 0.83\ J\ g^{-1}\ K^{-1}$.

The volumetric heat capacity s of a material results from:

$$s = c * \rho, \tag{S2}$$

with ρ being the density of the material. With a density of $\approx 3\ mg\ cm^{-3}$ the volumetric heat capacity is calculated as 2.5 $kJ\ m^{-3}\ K^{-1}$.

Supplementary Note 5 – Calculation of specific surface area

The high specific surface area of aeroglass is crucial for the heat transfer to the gas phase. Due to the lightweight and highly porous macroscopic structure standard techniques to determine the gravimetric surface area, such as BET, are difficult to apply, because the overall amount of material per volume is very low. Therefore, the specific surface area is estimated by the following calculation.

As the fabrication process is based on a template based approach, first the volumetric surface area (VSA) of the sacrificial tetrapodal ZnO (t-ZnO) template is calculated. For this, it was assumed that the ZnO tetrapods are composed of 4 rods with a diameter d = 2 µm and a length l of 25 µm.

The surface area of a single ZnO tetrapod $A_{tetrapod}$ is calculated by:

$$A_{tetrapod} = 4 * \frac{2\pi * \frac{d}{2} * \left(\frac{d}{2} + l\right)}{10^8} \tag{S3}$$

Knowing the template geometries ($V_{template}$), the density of the template ($\rho_{template}$ = 0.3 g cm^{-3}) and the density of ZnO (ρ_{ZnO} = 5.61 g cm^{-3}), the number of ZnO tetrapods $n_{tetrapods}$ per volume and the surface of tetrapods per volume $VSA_{template}$ can be calculated:

$$V_{tetrapod} = 4 * \frac{\pi * (\frac{d}{2})^2 * l}{10^{12}} \tag{S4}$$

$$n_{tetrapods} = \frac{V_{template} * \rho_{template}}{V_{tetrapod} * \rho_{ZnO}} \tag{S5}$$

$$VSA_{template} = \frac{A_{tetrapod} * n_{tetrapods}}{V_{template}} \quad \text{(S6)}$$

As the microstructure of aeroglass is composed of hollow microtubes, the VSA_{AG} can be estimated to be twice as the VSA of the template.

$$VSA_{AG} = 2 * VSA_{template} \quad \text{(S7)}$$

For microtubes with a rod diameter of 2 µm this results in:

$$VSA_{AG}(2\mu m) = 0.223 \frac{m^2}{cm^3} \quad \text{(S8)}$$

The gravimetric surface area GSA is calculated using the AG density ρ_{AG} = 3 mg cm^{-3}:

$$GSA_{AG} = \frac{VSA_{AG}}{\rho_{AG}} \quad \text{(S9)}$$

For microtubes with a rod diameter of 2 µm this results in:

$$GSA_{AG}(2\mu m) = 74.153 \frac{m^2}{g} \quad \text{(S10)}$$

Supplementary Note 6 – Calculation of surface area 2D vs. 3D

Assuming an ideal flat 2D surface with a radius of 6 mm, the surface area A_{2D} is calculated by:

$$A_{2D} = \pi\ 0.6\ cm^2 = 1.13\ cm^2 \quad \text{(S11)}$$

Considering a cylindrical aeromaterial sample with radius 6 mm and a height of 4 mm, the surface area A_{3D} can be calculated using equations S3 and S5, assuming a tetrapod diameter of 2 µm and a flat surface of the SiO_2 microtubes:

$$A_{3D} = A_{tetrapod} * n_{tetrapods} = 503.19\ cm^2 \quad \text{(S12)}$$

Supplementary Videos

Video 1

Concept of light induced volumetric gas activations in AG/rGO framework structures demonstrated by a gas micro pump. The gas activation (heating) results in a volume expansion, creating a directional flow through the check valves, as visualized by a droplet of dyed water which is pushed through a connected glass tube. The AG/rGO transducer material is illuminated with a frequency of 0.5 Hz as well as 1 Hz and with an irradiance of 1.24 W cm^{-2}.

Video 2

Demonstration of AG/rGO framework structure as transducer material for applications in light triggered pneumatic (untethered) soft robotics.

Video 3

Demonstration of AG/rGO framework structure as transducer material for the application as a light powered membrane pump for fluids.

References

(1) Malis, T.; Cheng, S. C.; Egerton, R. F. EELS log-ratio technique for specimen-thickness measurement in the TEM. *Journal of electron microscopy technique* **1988**, *8* (2), 193–200. DOI: 10.1002/jemt.1060080206.

(2) Iakoubovskii, K.; Mitsuishi, K.; Nakayama, Y.; Furuya, K. Thickness measurements with electron energy loss spectroscopy. *Microscopy research and technique* **2008**, *71* (8), 626–631. DOI: 10.1002/jemt.20597.

(3) Bell, N. C.; Minelli, C.; Tompkins, J.; Stevens, M. M.; Shard, A. G. Emerging techniques for submicrometer particle sizing applied to Stöber silica. *Langmuir : the ACS journal of surfaces and colloids* **2012**, *28* (29), 10860–10872. DOI: 10.1021/la301351k. Published Online: Jul. 11, 2012.

(4) Schütt, F.; Zapf, M.; Signetti, S.; Strobel, J.; Krüger, H.; Röder, R.; Carstensen, J.; Wolff, N.; Marx, J.; Carey, T.; Schweichel, M.; Terasa, M.-I.; Siebert, L.; Hong, H.-K.; Kaps, S.; Fiedler, B.; Mishra, Y. K.; Lee, Z.; Pugno, N. M.; Kienle, L.; Ferrari, A. C.; Torrisi, F.; Ronning, C.; Adelung, R. Conversionless efficient and broadband laser light diffusers for high brightness illumination applications. *Nature communications* **2020**, *11* (1), 1437. DOI: 10.1038/s41467-020-14875-z. Published Online: Mar. 18, 2020.

(5) Wang, L.; Tan, Z.; Meng, S.; Druzhinina, A.; Varushchenko, R. A.; Li, G. Heat capacity enhancement and thermodynamic properties of nanostructured amorphous SiO2. *Journal of Non-Crystalline Solids* **2001**, *296* (1-2), 139–142. DOI: 10.1016/S0022-3093(01)00902-4.